THE AMERICAN SOCIETY OF MECHANICAL ENGINEERS
345 E. 47th St., New York, N.Y. 10017

96-GT-233

APPLICATION OF ADVANCED EXPERIMENTAL TECHNIQUES IN THE DEVELOPMENT OF A COOLED TURBINE NOZZLE

H.K. Moon and B. Glezer
Aero/Thermo and Performance Analysis
Solar Turbines Incorporated
San Diego, California

ABSTRACT

In spite of very significant progress in analytical and numerical methods during recent years, experimental techniques are still essential tools for the development of cooled turbine nozzles. This paper describes the major elements of the development process for cooled turbine nozzles with a primary emphasis on advanced experimental heat transfer techniques. Thermochromic liquid crystals were used to measure the internal (coolant side) heat transfer coefficients of a practical vane cooling design which has a combination of different heat transfer augmenting devices. A comparison of the results and analytical predictions provided validations of existing correlations which were developed from the generic cases (usually one type of augmenting device). The overall cooling design was evaluated in a full-scale annular hot cascade which maintained heat transfer similarity. The freestream turbulence level was measured with an in-house developed heat flux probe. Cooling effectiveness distribution was evaluated from the surface metal temperatures mapped with an in-house developed wide range temperature pyrometer. The test results led to the fine-tuning of the nozzle vane cooling design.

NOMENCLATURE

Symbols

A	area
C	chord
D	diameter
h	heat transfer coefficient
t	time
T	temperature
V	velocity
W	mass flow rate
x	curvilinear distance
α	thermal diffusivity
γ	specific heat ratio
η	cooling effectiveness
τ	time step
θ	angle, degree
c_p	specific heat
Ec	Eckert number
Gr	Grashof number
Ma	Mach number
Pr	Prandtl number
Re	Reynolds number
Tu	percent turbulence intensity
C_{TU}	multiplier to account for freestream turbulence

Subscripts

a	aperture
b	bulk
c	coolant
comb	combustor
D	diameter
g	gas
i	initial
m	mixed mean
in	inlet
int	internal
s	surface
t	total
w	wall
∞	freestream
o	external

INTRODUCTION

The main objective of a turbine nozzle cooling design is to provide long component life (durability) at high turbine inlet temperatures using minimum cooling air. Minimizing of cooling air serves an even more critical role as the engine emission characteristics are becoming a primary concern for industrial engines and the cooling air saved from turbine component cooling can be used to improve combustor emission (Lefebvre, 1995). In order to have an effective cooling design, it is necessary to accurately predict the metal temperatures. Underprediction of metal temperature by as little as 17°C can result in the reduction of component

Presented at the International Gas Turbine and Aeroengine Congress & Exhibition
Birmingham, UK — June 10-13, 1996

oxidation life by 50% and may limit the creep-rupture life to one-quarter of the design life target (Hucek, 1985). The prediction of cooled turbine airfoil temperature distributions continue to present an ongoing design challenge. In spite of a tremendous progress in numerical methods during the recent years, both external (gas side) and internal (coolant side) heat transfer are still difficult to predict. The difficulties of external heat transfer prediction are attributed to the complex nature of nozzle vane external boundary conditions which include the effect of curvature, freestream turbulence, surface roughness, film cooling, secondary flow phenomena near the endwalls, etc. The internal heat transfer coefficient is often predicted from experimental correlations which have been developed from generic cases (usually comprised of one type of augmenting device). The internal heat transfer coefficient test data, however, is scarce for practical designs which have a combination of heat transfer augmenting devices (Abuaf and Kercher, 1994). For these reasons, the experimental validation of a cooling design remains an essential part of the development cycle for advanced turbine nozzles.

The present paper presents the application of modern experimental techniques to the development nf cooled turbine vanes. The internal (coolant side) heat transfer coefficients were measured with a Thermochromic Liquid Crystal (TLC) technique in a 7X scaled acrylic model. A hot cascade with an in-house developed turbulence probe provided heat transfer similarity to a full scale test nozzle. The cooling effectiveness distribution was evaluated from the surface metal temperatures measured with an in-house developed wide range temperature pyrometer. The analytical predictions of the external and internal heat transfer coefficients for a given airfoil design are presented along with the cooling design. The experimental results are compared to the analytical predictions.

COOLING DESIGN

Fig. 1 shows a typical interactive process in the development cycle of cooled turbine airfoils (Glezer, 1992). The process starts with a concept selection and analytical predictions of flows and temperatures, and ends with validations in hot cascade and engine tests. This paper begins with the heat transfer analysis and assumes that all other necessary information to carry out the cooling design of a nozzle vane are given. In reality, these other aspects are rarely fixed and the cooling design should be reconsidered accordingly. The chord length of the present nozzle vane is 5.8 cm. The Reynolds number and Mach number based on the exit conditions are 2.9 x 10^5 and 0.74, respectively. The freestream turbulence intensity of 12% is expected at the turbine inlet.

The cooling design of a nozzle is commonly based on conditions at the midspan where the local gas temperature is anticipated to attain a maximum value. The maximum gas temperature, $T_{g,max}$, is calculated at the turbine inlet from the pattern factor for a specific combustor:

$$PF = \frac{T_{g,max} - T_{g,mean}}{\Delta T_{comb}} \qquad (1)$$

where ΔT_{comb} specifies the temperature rise across the combustor. The pattern factor is an important parameter for stationery components, to directly assess the uncertainty in the local maximum gas temperature. The required metal temperature and wall thickness are determined from the life cycle requirements before the heat transfer analysis begins. Once the airfoil shape is determined and the associated pressure and velocity profiles are available, the external (gas side) convective heat transfer coefficients are computed in order to evaluate the cooling load. Based on the predicted heat load, the cooling techniques necessary to adequately cool the nozzle are determined from a cooling effectiveness chart, where the cooling effectiveness (defined below) is plotted against cooling parameter, $A_s h_c / W c_p$, or relative coolant flow ratio, W_c/W_g, for various cooling techniques, such as convection (turbulators and pin-fins), convection/impingement and convection/ impingement/film cooling:

$$\eta = \frac{T_g - T_{bw}}{T_g - T_{c,in}} \qquad (2)$$

For the present design effort, three different methods were used to predict the external convective heat transfer coefficients: the turbulent flat plate solution, BLAYER (McNally, 1970) and STAN5 (Crawford and Kays, 1976). BLAYER uses "integral" methods to provide the solution of the two-dimensional, compressible laminar and turbulent boundary layer equations in an arbitrary pressure gradient. All the results are plotted in Fig. 2. Since the nozzle coolant air of the present cooling configuration (stage one nozzle with primarily internal convection and air discharge through or near the trailing edge) does not substantially penalize the engine performance, the highest local predictions in Fig. 2 have been used in the present cooling design to be conservative: the cylinder in cross-flow solution in the vicinity of the leading edge and the modified BLAYER solution for the rest except the trailing edge on the suction side where the flat plate solution has been used. The BLAYER solution on the suction side was modified as shown in Fig. 2 based on the comparison to the other solutions and the past experience.

The transition from the laminar flow to the turbulent flow was assumed to occur immediately for BLAYER to be conservative. In order to assess the conservativeness inherent with BLAYER, a momentum thickness Reynolds number of 100 for the suction side and 60 for the pressure side was assumed for the transition in the STAN5 computation. STAN5 is expected to provide the overall most reliable solution for the present problem. Although it is not presented, STAN5 with immediate transition did not significantly change the maximum value but did change the location at which it occurred. The surface roughness and the initial turbulence level of the flow were not taken into account by either BLAYER or this version of STAN5. Since none of the above methods adequately predicts heat transfer coefficients in the vicinity of the leading edge, the cylinder in cross flow solution was modified to include turbulence effects. A constant multiplier, C_{Tu}, was used to account for the freestream turbulence.

Integrating the external heat transfer coefficient over the airfoil surface for given coolant supply conditions, the type of cooling design to meet the metal temperature requirements were determined from the cooling effectiveness chart. It was decided that the cooling air would be discharged through a row of slots on the pressure side to minimize the trailing edge thickness. A thin trailing edge is highly desirable not only for reasons of aerodynamic performance but also to reduce the generation of eddies at the downstream (blade) where the heat transfer is augmented. Assuming a certain wall thickness, the internal cooling requirements (or heat transfer coefficients) were calculated. The cooling configuration was then selected to meet the external airfoil heat load. After several iterations, the cooling configuration design was finalized as shown in Fig. 3. The external adiabatic wall temperatures were modified to include local film cooling. The cooling configuration utilizes a single insert, with cooling air being supplied through the outer support structure. Air impinges at the leading chordwise direction around the pressure and suction surfaces. Cooling is enhanced by the use of chordwise ribs and pin-fins, the geometric details of which are tailored to counterbalance the external airfoil heat load. The pressure surface cooling flow exits through a row of film holes, the location of which is controlled by the external static pressure distribution and the need to maintain an adequate margin to prevent hot gas ingestion. On the suction edge and forward suction surface, then the spent coolant flows in a

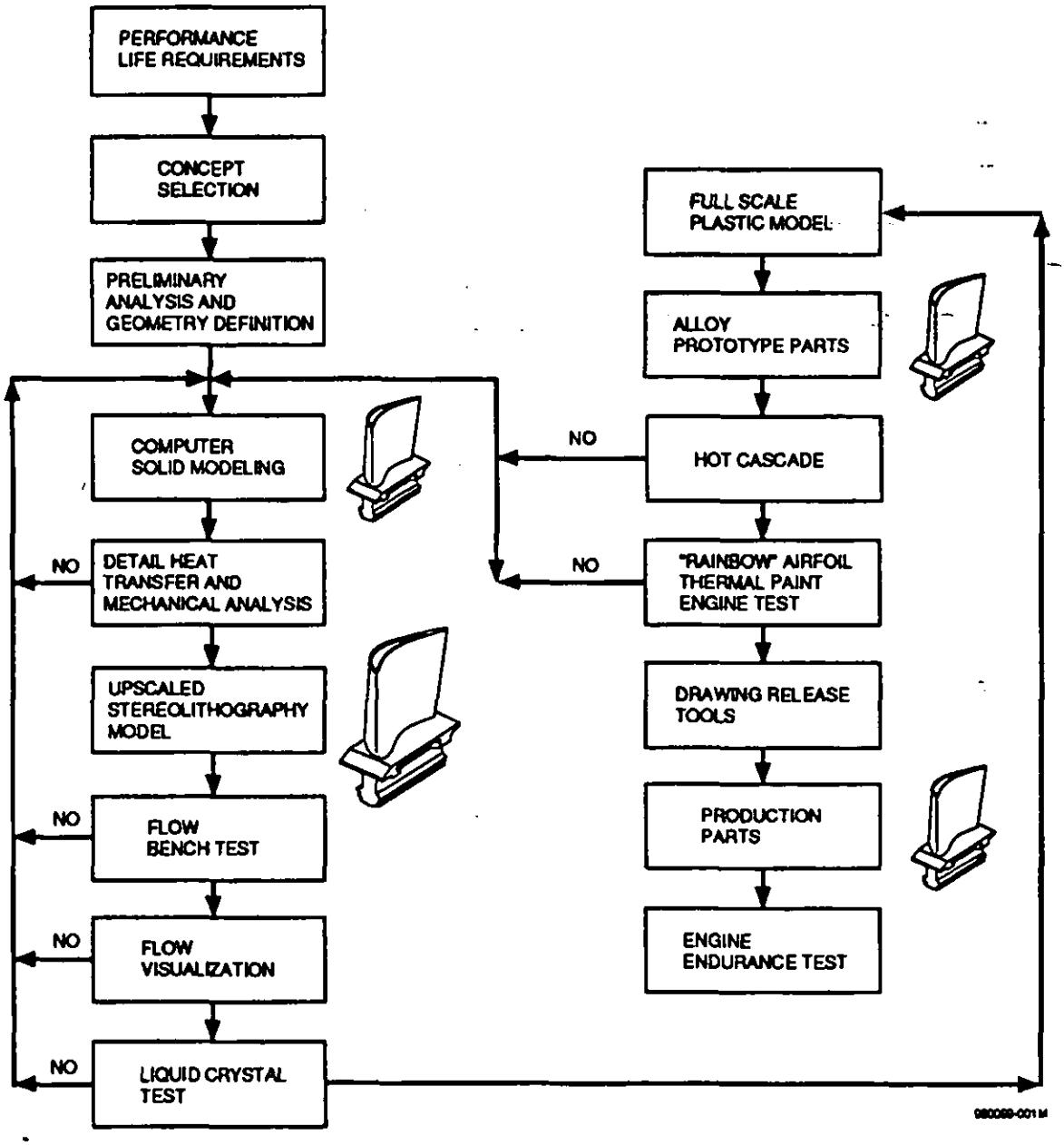

FIG. 1 - AIRFOIL COOLING DEVELOPMENT PROCESS

side, there is a row of diffusion holes which is designed to help the film adhere to the airfoil surface in this area of high curvature. This film provides a significant amount of cooling on the suction surface. Internal cooling flow around the suction surface continues through banks of pin-fins and exits at the trailing edge through pressure side slots. Cooling air dilution holes are provided towards the rear of the insert on the suction side as a means of reducing the local cooling air temperature. The design also utilizes a seal aft of the pressure surface film holes which allows for the control of the pressure/suction side flow split.

The internal heat transfer coefficients and coolant temperatures were calculated by an in-house flow network program. The step-changes in the heat transfer distribution as shown in Fig. 4 result from the experimental correlations which provide average values for the sections. On the pressure side, the inner wall in contact with the insert was modeled with an equivalent convection boundary. The equivalent heat transfer coefficients for the projected wall were calculated for the film cooling holes, pressure side discharge holes, ribs, and pin-fins.

After both the external and internal boundary conditions were defined, an ANSYS™ finite element analysis was performed to obtain the surface metal temperature distribution. The surface metal temperatures were used to evaluate the cooling effectiveness instead of the bulk metal temperatures for convenience. The resulting cooling effectivenss distribution is plotted in Fig. 5.

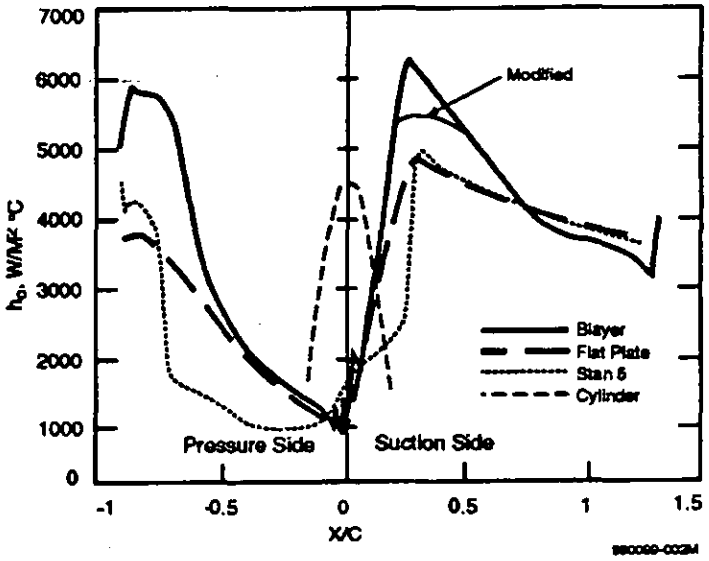

FIG. 2 - EXTERNAL HEAT TRANSFER COEFFICIENT DISTRIBUTION

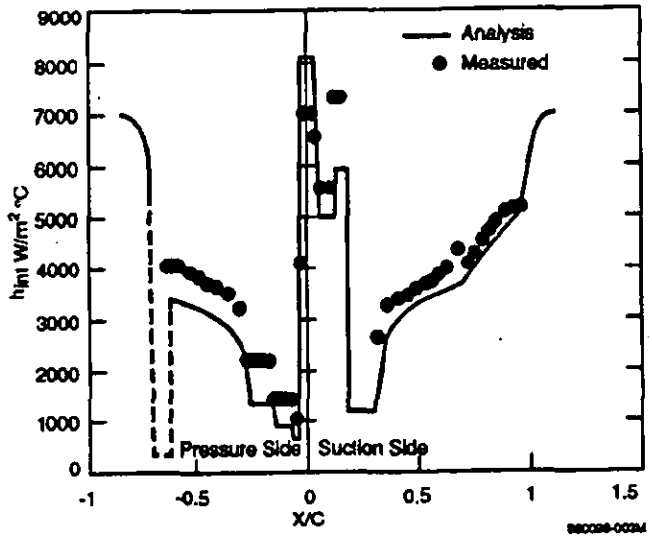

FIG. 4 - INTERNAL HEAT TRANSFER COEFFICIENT DISTRIBUTION

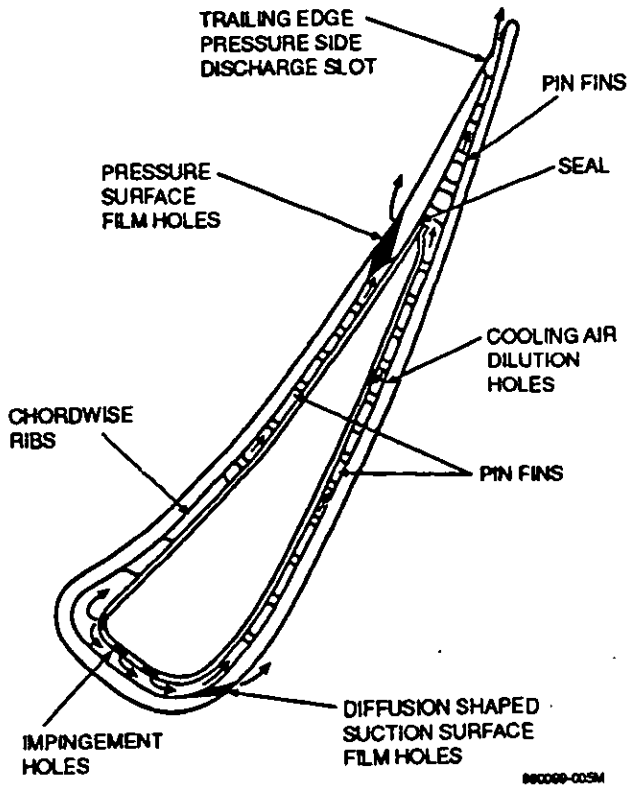

FIG. 3 - VANE AIRFOIL COOLING CONFIGURATION

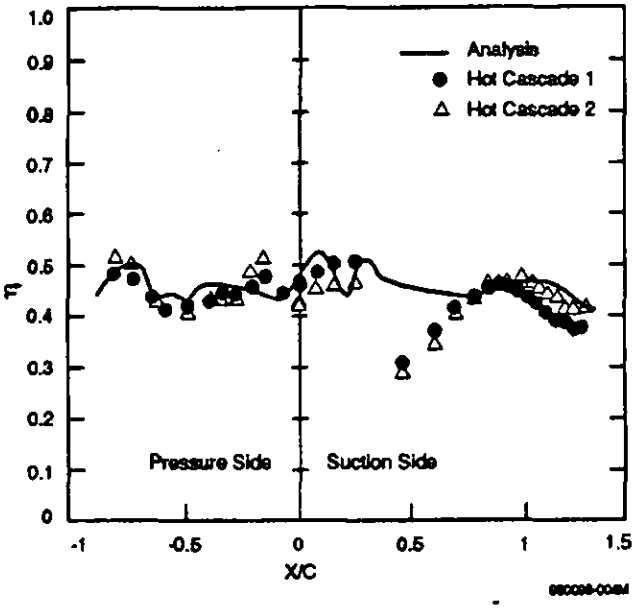

FIG. 5 - COOLING EFFECTIVENESS DISTRIBUTION

EXPERIMENTAL DESIGN VERIFICATION

Experimental verification with advanced heat transfer measurement techniques plays an important role in cooling design process. In the present study, the internal heat transfer coefficient and cooling effectiveness distributions were measured and compared to the predicted values.

Internal Heat Transfer Measurements with TLC

In recent years, thermochromic liquid crystals have been used to measure heat transfer coefficients by a number of researchers as the state-of-the art image processing technology becomes available. Since Ireland and Jones (1986) applied liquid crystals to the transient technique previously used with melting material (Larson, 1983) for measuring local heat transfer coefficients in blade cooling geometries, the transient liquid crystal technique has been extensively used for gas turbine heat transfer measurement. The transient technique is relatively simple and inexpensive compared to the steady state technique (Hippensteele and Russell, 1984, and Baughn et al., 1989). There are several methods to identify the liquid

crystal coated surface temperature during the transient experiments. Camci and Kim (1992) utilized a hue capturing technique to quantitatively interpret the liquid crystal images. Wang (1993) introduced a method based on the optical signal pattern during the transient experiments. The present experiment utilized the change in the decomposed green signal to identify the surface temperature (Kim and Metzger, 1993) to validate the analytical predictions of cooled turbine vane internal heat transfer coefficients in an up-scale acrylic model.

The temperature dependent color display characteristics of thermochromic liquid crystal (TLC) was utilized in the present measurement of internal convective heat transfer coefficients, which is similar to the techniques reported by Metzger and Larson (1986), and Vendula, et al. (1988). Knowing the green signal level versus temperature, the time required for the local surface temperature to reach a predefined value after it is suddenly exposed to a hot gas was measured. The transition time distribution was then converted to the heat transfer coefficient using the following semi-infinite medium solution:

$$\frac{T - T_i}{T_m - T_i} = 1 - \exp\left(\frac{h^2 \alpha t}{k^2}\right) erfc\left(\frac{h\sqrt{\alpha t}}{k}\right) \qquad (3)$$

In actual internal experiments, the wall surfaces do not experience a pure step change in air temperature because of the transient heating of the upstream walls. Nevertheless, equation (4) is a fundamental solution that can be used to represent the response to a superposed set of elemental steps in T_m arranged to represent the actual air temperature rise:

$$T - T_i = \sum_{i=1}^{N} U(t - \tau_i)\, \Delta T_m \qquad (4)$$

where

$$U(t - \tau_i) = 1 - \exp\left[\frac{h^2 \alpha (t - \tau_i)}{k^2}\right] erfc\left[\frac{h\sqrt{\alpha (t - \tau_i)}}{k}\right]$$

An overall schematic view of the test setup is shown in Fig. 6. The test apparatus consisted of the test section, air-supply system, thermal data acquisition system and imaging processing system. The test section, scaled to 7X, was constructed from a transparent acrylic to allow viewing from the outside (see Fig. 7). The surface of the test section on which the heat transfer coefficients were to be measured, were first coated with the TLC (Hallcrest, R35C1W) and then spray-painted black (Hallcrest, BB-G1) to provide an optimum contrasting visual background for the liquid crystal color display. The compressed air was filtered and dried before supplied to the test rig. The air was heated with an inline electric heater with automatic temperature controlled power input. A pneumatic three-way diverter was used to bypass the heated air from the test section until the heated air reached the desired temperature. Aero/thermal data such as temperatures and pressures were acquired by a MicroVax and Daytronic-based system. The image processing system included a Y-C camera (Cohu 8210) and a Silicon Graphics Indy workstation (R4000SC). A diffused light was mounted on the camera to reduce the view-angle dependency of the TLC color transition as discussed by Herold and Wiegel (1980). Furthermore, the TLC was calibrated with a coupon at the representative angle at the beginning of each test.

The leading edge, pressure side and suction side tests (a total of six camera views) were conducted independently of each other in order to ensure correct flows (Reynolds numbers) under atmospheric condition as

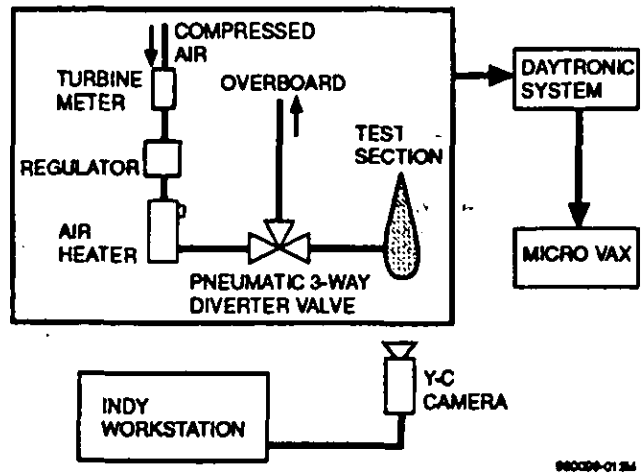

FIG. 6 - SCHEMATIC VIEW OF IMAGING TEST APPARATUS

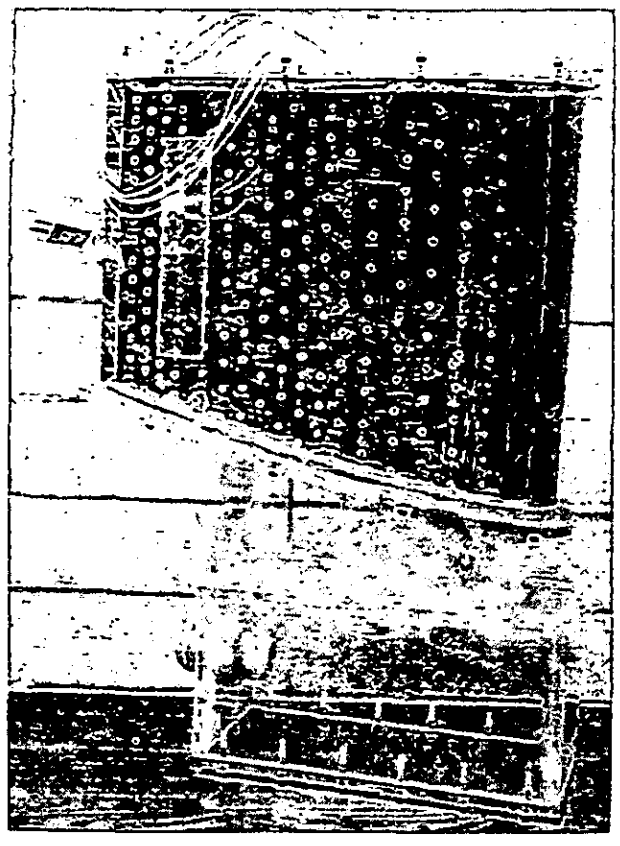

960099-011M/S

FIG. 7 - LIQUID CRYSTAL COATED TEST VANE

predicted with an in-house flow network program, rather than by simulating the engine external static pressure distribution over the airfoil. Figure 8 shows the forward suction side results of the TLC measurement before scaling back to account for the test model size, which clearly show heat transfer augmentations by pin-fins. Measured average heat transfer coefficients in streamwise direction are plotted in Fig. 4 and compared to the

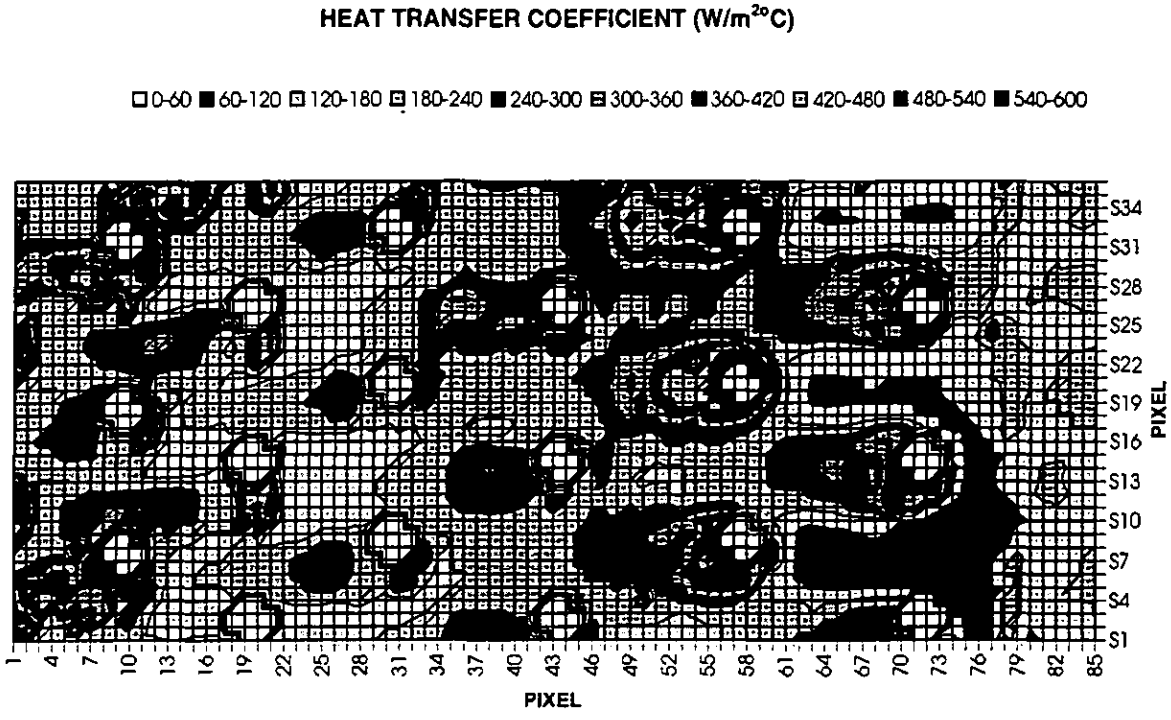

FIG. 8 - TYPICAL LIQUID CRYSTAL TEST RESULT

predicted values. The measured values are generally higher than the predicted values. This is probably due to either of two reasons. First, the predictions were made based on a flat coolant velocity profile in the vane coolant although the measurements were conducted at the middle one-third of the vane height where the velocity was expected higher than the average. The second possible explanation is due to the higher turbulent level after impingement. The measured impingement heat transfer coefficients on the suction side are consistently higher than the predicted values. This may have been due to over-estimated cross flow effects in the correlation used in the analysis. To conclude, the present measurements demonstrated the liquid crystal technique to be an effective tool to validate analytical predictions in the gas turbine cooling design cycle.

Heat load and Cooling Effectiveness Simulation in Hot Cascade

Realistically simulated steady-state hot cascade experiments using actual engine hardware with proper external/internal cooling arrangements are extremely beneficial for evaluating turbine vanes in the early stage of turbine development (Hiroki and Katsumata, 1974).

The cooling effectiveness of the nozzle vane was evaluated in the hot cascade by simulating the forced convection in the engine based on a number of dimensionless groups in a nondimensionalized form of the Navier-Stokes and energy equations for a compressible fluid (Glezer et al., 1994). The nondimensional parameters have been identified as Re, Gr/Re^2, $1/(PrxRe)$ and Ec in the past (Schmidt (1963), Eckert and Drake (1972), Schlichting (1979)). For most of the forced convection problems such as external heat transfer of a turbine nozzle vane, buoyancy forces are considered negligible compared to inertial forces. Therefore, the Grashof number, Gr, is neglected in the present study. The Eckert number, Ec, can be expressed in terms of freestream Mach number, Ma, wall to gas temperature ratio, T_w/T_g and the specific heat ratio, γ:

$$Ec = (\gamma-1)\, Ma^2 \frac{\dfrac{1}{1 + \dfrac{(\gamma-1)}{2} Ma^2}}{1 - \dfrac{T_w}{T_{tg}}} \qquad (5)$$

Therefore, simulation of the forced convection heat transfer process in a gas turbine vane surface requires the similarity of Re, Pr, Ma, T_w/T_g, γ. It should be noted that these similarity parameters result from the laminar/unsteady form of the momentum and energy equations. In addition, the freestream turbulence, Tu, also effects airfoil heat transfer and should be replicated during heat transfer simulation experiments.

Similarity principles applied to the gas side of the hot cascade can be also implemented for the coolant (air) side of the airfoil. Once the gas side conditions are selected for the hot cascade, the total coolant temperature is calculated by matching the ratio of total coolant to freestream temperature to that of the engine. The coolant mass flow rate is adjusted to match the coolant Reynolds number of the engine. In the present hot cascade experiment, Re, Ma, and T_w/T_g for the gas side, and Re and T_w/T_c for the coolant side were matched for heat transfer similarity. In addition, the freestream turbulence level was also measured.

A schematic of the test rig is shown in Fig. 9. It features a full-scale annular cascade to provide geometric similarity. A natural gas fueled can combustor (the actual engine employs a larger size annular combustor) was used to support the automated hot cascade operation for a wide range of pressures, flows and temperatures. Compressed air and gas were supplied at about room temperature from the central factory source. Air flow was measured with a turbine flow meter and established by a remote-controlled regulator. A radially inserted electric igniter ensured the combustor light off

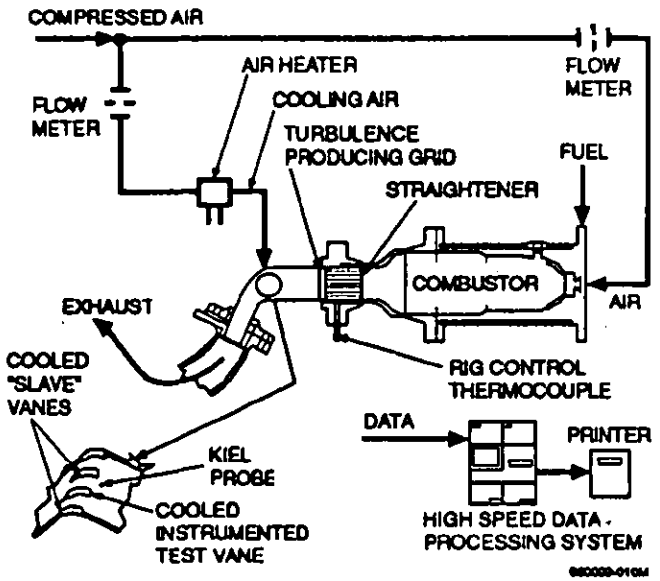

FIG. 9 - HOT CASCADE TEST RIG

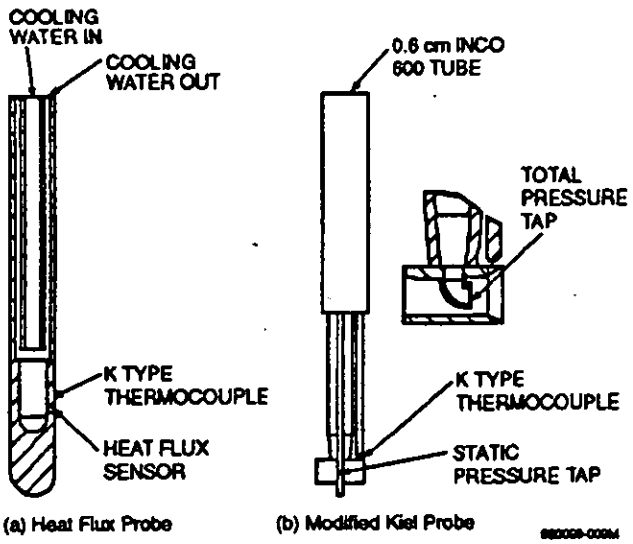

FIG. 10 - SCHEMATIC OF (a) HEAT FLUX PROBE AND (b) MODIFIED KIEL PROBE

and supported ignition even at relatively low fuel/air ratios. The hot cascade accommodated four vanes including two "slave", internally cooled vanes, to provide the central test vane with radiation and aerodynamic similarities. The coolant air supplied to all three vanes of the hot cascade was electrically heated to maintain gas to cooling air temperature ratio. The combustor exit temperature was controlled with dilution air, and the combustor pressure was controlled by a throttle valve positioned downstream of the hot cascade. The type of grid situated at 28 cm upstream of the test section controlled the turbulence level.

The turbulence intensity was indirectly measured with the methodology discussed by Zhang and Glezer (1995). The custom-designed heat flux probe and Kiel probe which were used in the present study to measure stagnation heat transfer on circular cylinder and corresponding Reynolds number in hot cascade condition are shown in Fig. 10. Turbulence intensity was estimated based on the following correlation of stagnation heat transfer with turbulence intensity and Reynolds number, which was slightly modified from the Lowery and Vachon (1975) correlation:

$$\frac{Nu_D}{\sqrt{Re_D}} = 1.01 \left(\frac{Re_D}{100{,}000}\right)^{0.05} + 0.058 \left(Tu\sqrt{Re_D}\right)^{0.65} \qquad (6)$$

The turbulence intensity of 12% was estimated at the test section inlet with the grid used in the present hot cascade test. Without the grid, the turbulence intensity was limited to 6%.

Surface Temperature and Cooling Effectiveness Mapping with Pyrometer

The surface temperatures of the test vane were measured with the in-house developed pyrometer which has been validated in a previous study (Moon et al., 1995). The pyrometer has a lower surface temperature limit of 230°C unlike commercially available pyrometers that can only measure temperatures above 600°C. Figure 11 shows a schematic cut-away view of the probe. The housing holds the optical core assembly and redirects incoming radiation by ninety degrees with a gold alloy mirror. The bore extension of the housing is the part that actually protrudes into a gas stream and includes the first aperture, whose diameter is 3.66 mm, to form a collimated field of view. The housing has an air port. The supply air is provided to cool the tapered optical fiber, which has an operating temperature limit of 100°C, and also to keep the exposed optical system clean by purging. A cooling chamber is provided between the housing and the optical core in which two sets of four forced convection fins are located. Pressurizing the probe also prevents hot gas ingestion and cools the mirror to reduce radiation emission. The optical core contains a tapered fiber made of a material called chalcogenide and tapered from a diameter of 3 mm to a diameter of 1 mm. One end (1 mm diameter side) of the optical core is equipped with a cable adapter. The other end is finished with an end cap. A sapphire lens is displaced within the end cap in such that the wide end of the tapered fiber is one focal length (10 mm) away from it. The end cap includes the second aperture whose diameter is 3.66 mm. A K-type thermocouple was installed on the optical core near the end cap to ensure the tapered fiber temperature is under its operating temperature limit. The

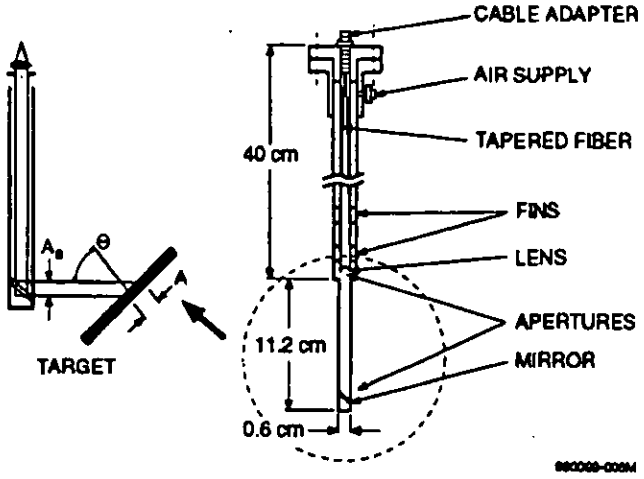

FIG. 11 - CUT-AWAY VIEW OF THE PYROMETER

optical probe was connected to the detector via an IR optical cable. The IR optical cable has a fiber core, 1 mm in diameter. Two types of IR optical cable, chalcogenide and fluoride, were available for the experiment, but the fluoride cable was used for the present experiment because of its less fragile nature. The detection system consisted of a detector and signal conditioner. The detector had a wavelength window of 2.0 to 2.25 μm, thus avoiding the absorption bands of the gases commonly present in combustion products. The transmission losses of the chalcogenide and fluoride fibers were 0.27 dB/m and 0.025 dB/m respectively at this wavelength window. The electrical signal from the detector was conditioned and linearized to a target temperature in the signal conditioner, generating the voltage output linearly proportional to the target temperature. The signal conditioner had a target emissivity setting knob which controlled the signal gain factor.

The pyrometer is not only convenient when compared to thermocouples but also it is able to map the surface temperature distribution. The test vane was instrumented with four thermocouples at the mid-span, buried flush into the wall to provide an aerodynamically smooth surface. The thermocouples provided reference temperatures for the pyrometer. The pyrometer was mounted in a traversing device with both rotational and axial freedoms to scan the mid-section of the test vane. An overall view of the pyrometer test apparatus is shown in Fig.12. The traversing device was digitally controlled to provide an accurate linear movement with a spatial resolution of 0.02 mm and to be rotated with a resolution of 0.01 degree to maximize viewing of the nozzle surface. As shown in Fig. 13, the test vane surface at mid-section was scanned in an increment of 5 degrees from three different pyrometer access ports.

The hot cascade tests were conducted at gas temperatures of 480°C and 540°C and the cooling effectiveness results based on the surface metal temperatures are plotted against the predictions in Fig. 5 (HOT CASCADE 1 and HOT CASCADE 2, respectively). The test data shows a relatively flat cooling effectiveness near the leading edge on the suction side implying that the minimum external heat transfer coefficient on the suction side near the leading edge ($x/C \simeq 1$) is not as low as predicted. The large deviation immediately following the film cooling holes may have been caused by the film coolant being heated up more than anticipated before exiting into the gas stream. It is also possible that due to the surface convex curvature of the vane immediately following the discharge holes and the high turbulence level, film cooling was locally less effective than predicted. The test results on the pressure side were matched by predictions within 15% in spite of the conservative external heat transfer approach. Knowing that the internal heat transfer coefficients were measured and are somewhat higher than predicted, the hot cascade results demonstrated that the conservative external heat transfer prediction was a good design practice.

TUNED COOLING DESIGN

Regardless of what have caused the local ineffectiveness of the film cooling on the forward suction surface, the hot cascade test results showed room for improvements. It was decided to move the film cooling holes further downstream on the suction surface and redesign the impingement holes. These design changes only affect the impingement hole configuration of the insert and the locations of the film cooling holes. After several iterations between the ANSYS™ analysis and the flow network analysis, the cooling design was optimized to the configuration shown in Fig. 14. Five rows of impingement holes provide cooling for the leading edge and forward suction surface while keeping the coolant air flow rate and the surface metal temperatures under the design limit.

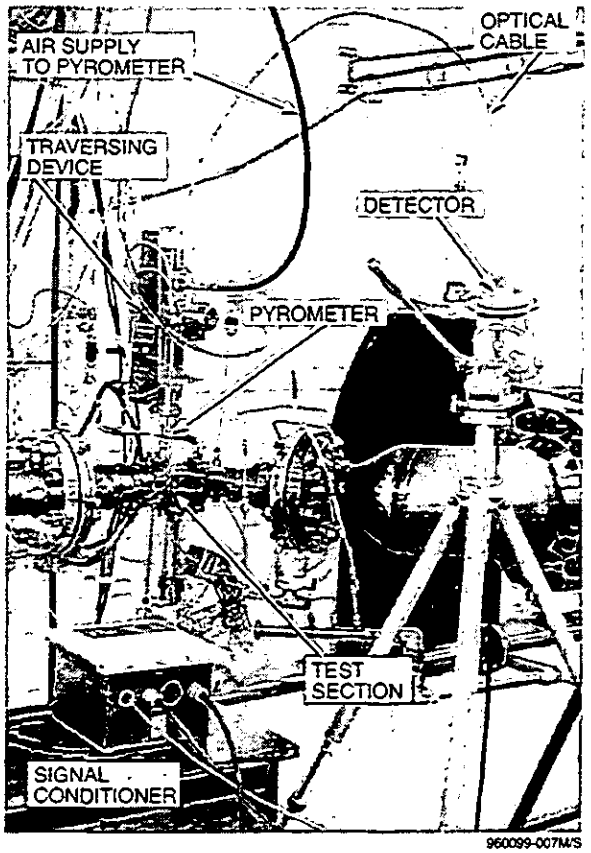

FIG. 12 - OVERALL VIEW OF THE PYROMETER TEST APPARATUS

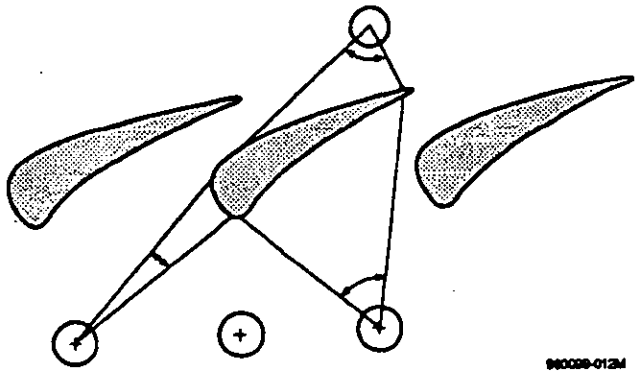

FIG. 13 - MID-SECTION VIEW OF THE TEST SECTION

CONCLUDING REMARKS

It has been demonstrated that experimental techniques play an essential role in the development of cooled turbine nozzles. Using experimental techniques to validate analytical predictions allows for the modification of existing design practices.

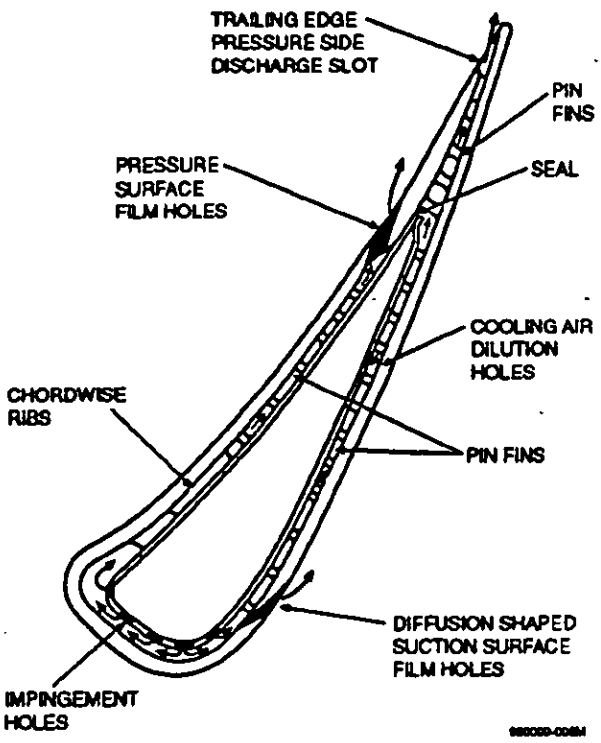

FIG. 14 - TUNED VANE AIRFOIL COOLING CONFIGURATION

A thermochromic liquid crystal technique was used to measure the internal heat transfer coefficients in a 7X scale model and validated the existing internal heat transfer correlations applicable to cooled turbine vane designs. A full-scale annular hot cascade provided the similarities of Re, Ma, T_w/T_g, and T_w/T_c. An in-house developed probe which simulated a realistic turbulence level in the hot cascade provided an additional control of the convective heat transfer similarity. The metal surface temperatures measured with the in-house developed wide range temperature pyrometer provided a detailed cooling effectiveness distribution.

REFERENCES

Abuaf, N. and Kercher, D.M., 1994, "Heat Transfer and Turbulence in a Turbulated Blade Cooling Circuit," Journal of Turbomachinery, Vol. 116, pp.166-177.

Baughn, J.W., Ireland, P.T., Jones, T.V., and Sanei, N., 1989, "A Comparison of the Transient and Heated-Coating Methods for The Measurement of Local Heat Transfer Coefficients on a Pin Fin," ASME Journal of Heat Transfer, Vol.111, pp. 877-881.

Camci, C., Kim, K. and Hippensteele, S.A., 1992, "A New Hue Capturing Technique for Quantitative Interpretation of Liquid Crystal Images used in Convective Heat Transfer Studies," Journal of Turbomachinery, Vol.114, pp. 765-775.

Crawford, M.E. and Kays, W.M., 1976, "STAN5 a program for numerical computations of two dimensional internal and external boundary layers," NASA CR-2742.

Eckert, E.R.C., and Drake, R.M., 1972, *Analysis of Heat and Mass Transfer*, McGraw Hill, pp. 389-397.

Glezer, B., 1992, "Some Aspects of Industrial Gas Turbine Cooling Development," International Symposium Heat Transfer in Turbomachinery, Athens, Greece.

Glezer, B., Moon, H.K., Zhang, L., and Camci, G., 1994, "Application of a Heat Flux/Calorimeter-Based Method To Assess The Effect of Turbulence on Turbine Airfoil Heat Transfer, ASME 94-GT-95.

Herold, W. And Wiegel, D., "Problems of the Photographic Documentation of Liquid Crystalline Thermographs," Advances in Liquid Crystal Research and Applications, L. Bata, ed.; Pergamon Press, Oxford, pp. 1255-1259.

Hippensteele, S.A., and Russell, L.M.,1984, "Use of a Liquid Crystal, Heater-Element Composite for Quantitative, High-Resolution Heat Transfer Coefficients On a Turbine Airfoil Including Turbulence and Surface Roughness Effects, TM 87355, NASA.

Hiroki, T. and Katsumata, I., "Design and Experimental Studies of Turbine Cooling," ASME 74-GT-30.

Hucek, H.J., 1985, *Aerospace Structural Metals Handbook*, Metals and Ceramics Information Center, Battelle's Columbia Laboratories.

Ireland, P.T. and Jones, T.V., 1986, "The Measurement of Local Heat Transfer Coefficients in Blade Cooling Geometries," AGARD Conference Proceedings on Heat Transfer and Cooling, CP 390, Paper 28.

Kim, Y.W., and Metzger, D.E., 1993, "Heat Transfer Effectiveness on Film Cooled Turbine Blade Tip Models," ASME 93-GT-208.

Larson,, D.E., 1983, "Transient Local Heat Transfer Coefficient Measurements in 90° Bends Using Surface Coatings Having Prescribed Melting Points," MS Thesis, Arizona State University.

Lefebvre, H., 1995, "The Role of Fuel Preparation in Low Emissions Combustion," ASME 95-GT-465.

Lowery, G.W., and Vachon, R.I., 1975, "The Effect of Turbulence on Heat Transfer from Heated Cylinders," International Journal of Heat and Mass Transfer, Vol. 18, pp. 1229-1242.

McNally, W.D., 1970, "Fortran Program for Calculating Compressible Laminar and Turbulent Boundary Layer in Arbitrary Pressure Gradients, NASA TND-5681.

Metzger, D.D. and Larson, D.E., 1986, "Use of Melting Point Surface coatings for Local Convection Heat transfer Measurements in Rectangular Channels with 90-degree Turns," J. of Heat Transfer, Trans. ASME, 1098, pp. 48-54.

Moon, H.K., Glezer, B., Mink, B. and Marvin, W., 1995, "Development of a Wide Range Temperature Pyrometer for Gas Turbine Application," ASME 95-GT-126.

Schmidt, E., 1963, *Einfurung in die Techniche thermodynamik und in die Grunlagen der Chemischen Thermodynmik*, 10th Ed., Berlin.

Schlichting, H., 1979, *Boundary Layer Theory*, 7th Ed., McGraw Hill, pp. 271-275.

Vendula, R.J., Metzger, D.D., and Bickford, W.B., 1988, "Effects of Lateral and Anisotropic Conduction on the Determination of Local Convection Heat Transfer", Collected Papers in Heat Transfer 1988, ASME, Heat Transfer div., Vol. 104, pp. 21-28.

Wang, Z., Ireland, P.T. and Jones, T.V., 1993, "An Advanced Method of Processing Liquid Crystal Video Signals from Transient Heat Transfer Experiments," ASME-GT-282.

Zhang, L. and Glezer B., 1995, "Indirect Turbulence Measurement in Gas Turbine Stages Using Heat Flux Probe," ASME-GT-153.